Supplementary Information for: Stepped frequency comb advanced sub-THz bandwidth spectrum sensing

Yang Yang[1], Zhiqiang Fan[1,]*, Jun Su, Yunxiang Wang, Shuangjin Shi, and Qi Qiu

School of Optoelectronic Science and Engineering, University of Electronic Science and Technology of China, Chengdu 610054, China.

*Correspondence authors: zqfan@uestc.edu.cn

[1]These authors contributed equally: Yang Yang, Zhiqiang Fan.

Supplementary Note 1: Comparison among SFC-based, parallel-channelization, and stepped-frequency serial-sweeping spectrum sensing systems

Supplementary Note 2: Theory of stepped frequency comb generation

Supplementary Note 3: Signal-to-noise ratio of the SFC

Supplementary Note 4: Generation of electro-optic comb

Supplementary Note 5: Optical injection locking of the distributed feedback laser diode

Supplementary Note 6: Image rejection of the SFC advanced spectrum sensing

Supplementary Note 7: Voltage-frequency characteristic of the voltage control oscillator

Supplementary Note 8: Numerically calculated spectrograms and captured spectra of various SUTs

Supplementary Note 1: Comparison among SFC-based, parallel-channelization, and stepped-frequency serial-sweeping spectrum sensing systems

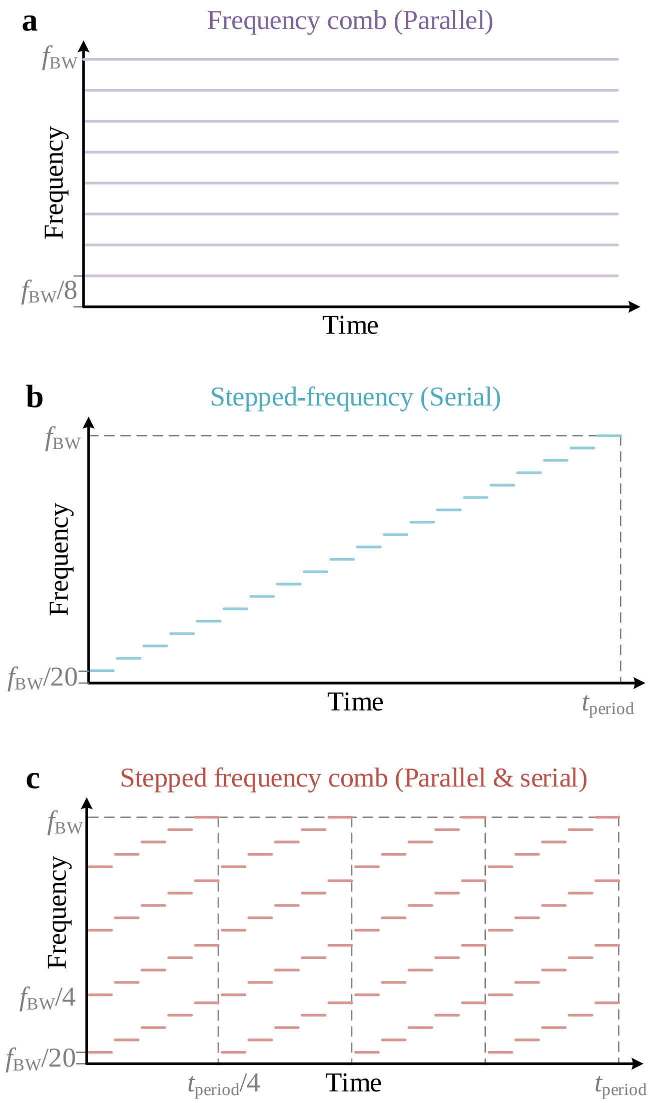

Fig. S1. Comparison of stepped frequency comb-, parallel-, and serial-based spectrum sensing systems. a, Parallel channelization. **b,** Stepped frequency serial sweeping. **c,** Stepped frequency comb.

A comparison among stepped frequency comb (SFC)-based spectrum sensing, parallel channelization, and stepped-frequency serial-sweeping spectrum sensing is shown in Fig. S1. Assuming the spectrum sensing system has a total receiver bandwidth of f_{BW}, these three schemes differ mainly in how they balance measurement bandwidth, frequency resolution, temporal resolution, and receiver hardware requirements.

For the parallel-channelization scheme, the measurement band is divided into multiple sub-channels that are processed simultaneously. If each sub-channel covers a bandwidth of $f_{BW}/8$, the system requires eight receiver units, each with a bandwidth of $f_{BW}/8$, as shown in Fig. S1a. Because all sub-channels are measured in parallel, the temporal resolution is mainly limited by the processing time of the receiver units rather than by serial sweeping. At the same time, the figure of merit (FOM), defined as the ratio of measurement bandwidth to frequency resolution, can remain high because the scheme preserves high frequency resolution across the full measurement process.

By contrast, the stepped frequency serial-sweeping scheme improves hardware efficiency by interrogating the spectrum sequentially. In this case, the number of the receiver unit and the required receiver bandwidth can be reduced to 1 and $f_{BW}/20$, respectively, as shown in Fig. S1b. This simplification, however, is achieved at the expense of temporal resolution, because the spectrum must be scanned step by step over one complete sweeping period. As a result, the temporal resolution is reduced to t_{period}.

The proposed SFC advanced spectrum sensing combines the FOM of parallel channelization with the receiver hardware efficiency of serial sweeping, as shown in Fig. S1c. By introducing stepped frequency operation within multiple parallel sub-channels, the scheme preserves efficient spectrum interrogation while improving the receiver hardware efficiency. Compared with the parallel-channelization method, the number of receiver units and the required receiver bandwidth are reduced to 4 and $f_{BW}/20$, respectively. Compared with the stepped frequency serial sweeping method, the temporal resolution is improved to $t_{period}/4$. Therefore, the proposed SFC scheme provides a more balanced solution, simultaneously offering high hardware efficiency, high temporal resolution, and a large FOM.

Supplementary Note 2: Theory of stepped frequency comb generation

Assuming the continuous wave (CW) laser in the SFC generation module is $E_0(t) = E_0 \exp(i2\pi f_0 t)$, where E_0 and f_0 are the amplitude and the frequency of the CW laser. The optical pulse signal from the acousto-optic modulator (AOM1) is expressed as

$$E_p(t) \propto \sum_n \mathrm{rect}\left(\frac{t - nT_s}{\tau_\mathrm{b}}\right)\exp\left[i2\pi\left(f_0 + f_\mathrm{b}\right)t\right] \quad \text{(S1)}$$

where τ_b is the pulse width of the optical pulse signal, T_s is the period of the optical pulse signal, and f_b is the frequency shift of the AOM1.

The optical pulse signal is injected into a recirculating frequency-shifted fiber loop (RFSFL), which consists of an erbium-doped fiber amplifier (EDFA), an optical bandpass filter (OBPF), and an AOM2 with the same frequency shift of f_b. The output of the RFSFL is expressed as

$$E_\mathrm{SF}(t) \propto g(f)\sum_{m=0}^{\mathrm{M}-1} \mathrm{rect}\left(\frac{t - mt_b}{\tau_\mathrm{b}}\right)\exp\left\{i2\pi\left[f_0 + (m+1)f_\mathrm{b}\right](t - mt_\mathrm{b})\right\} \quad \text{(S2)}$$

where M is the round-trip number and t_b is the loop delay of the RFSFL. $g(f)$ is the spectral envelope function determined by intra-loop components such as the OBPF and the EDFA, which is mapped to the temporal envelop window of the frequency-shifted pulses [S1]. To avoid interference between subpulses, the pulse width τ_b is less than the loop delay t_b, and the period T_s of the optical pulse signal equals $\mathrm{M}t_\mathrm{b}$.

The stepped frequency is connected to an electro-optic comb module to generate an SFC signal. The SFC signal can be expressed as

$$E_\mathrm{SFC}(t) \propto g_\mathrm{EO}(f)\,g(f)\sum_{n=0}^{\mathrm{N}-1}\sum_{m=0}^{\mathrm{M}-1} \mathrm{rect}\left(\frac{t - mt_b}{\tau_\mathrm{b}}\right)\exp\left\{i2\pi\left[f_0 + nf_\mathrm{ch} - \Delta f_\mathrm{ch} + (m+1)f_\mathrm{b}\right](t - mt_\mathrm{b})\right\} \quad \text{(S3)}$$

where $g_\mathrm{EO}(f)$ is the spectral envelope function determined by the electro-optic comb module. f_ch and N are the comb interval and the comb number of the electro-optic comb module. Δ is the comb number difference between the first comb tooth and the comb teeth at f_0.

In the experimental demonstration, the frequency shift f_b of the AOM1 and AOM2 is 200 MHz. The round-trip number and the loop delay t_b of the RFSFL are 250 and about 142 ns. A Mach-Zehnder modulator is used as the electro-optic comb module, and the comb interval f_ch and the comb number N are 50 GHz and 3. The comb number difference Δ is 1.

Supplementary Note 3: Signal-to-noise ratio of the SFC

For the signal-to-noise ratio (SNR) of the SFC, it is mainly limited by the stepped-frequency because of the amplified spontaneous emission (ASE) noise of the EDFA in the RFSFL. Hence, the SNR of the stepped frequency is discussed.

The input optical power P_{in} of the RFSFL is expressed as $P_{in} = P_0\tau_b / (Mt_b)$. For the first sub-pulse, the output optical power of the RFSFL is $P_1 = \alpha P_{in}$, where α is the coupled loss of the optical coupler. For the m^{th} sub-pulse ($m > 1$), the output optical power of the RFSFL is expressed as

$$P_m = (1-\alpha)^2 \alpha^{m-2} l^{m-1} g(f)^{m-1} P_{in} \tag{S4}$$

where l is the loss in the RFSFL.

After optoelectronic conversion, the power of each sub-pulse is expressed as

$$P_{RF-m} = \frac{1}{2}(P_m \Re)^2 R \tag{S5}$$

where $\Re$ is the photodiode responsivity, and R is the load resistance.

The m^{th} round-trip ($m > 1$) ASE noise power is expressed as

$$a_m = (1-\alpha)\sum_{k=2}^{m} \alpha^{k-2} l^{k-1} g(f)^{k-1} a_0 \tag{S6}$$

where the first round-trip noise a_1 power is assumed to be zero. a_0 is expressed as [S2]

$$a_0 = h\nu n_{sp}\left[g(f)-1\right] f_b \tag{S7}$$

where n_{sp} is the spontaneous emission factor ($n_{sp} > 1$), n_{sp} can be related to the noise figure of the EDFA by NF = 10 log($2n_{sp}$) [S3]. h and ν are respectively the Planck's constant and the central frequency of the photons ($\approx f_0$).

After optoelectronic conversion, the dominant noise source is the signal-spontaneous beat noise [S4], which is expressed as

$$P_{RF-s-sp} = 2\Re^2 R P_m a_m \tag{S8}$$

The SNR of the m^{th} sub-pulse ($m > 1$) of the stepped frequency generated in the RFSFL is expressed as

$$\mathrm{SNR}_m = \frac{P_{RF-m}}{P_{RF-s-sp}} = \frac{P_m}{4a_m} = \frac{(1-\alpha)\alpha^{m-2} l^{m-1} g(f)^{m-1} P_{in}}{4h\nu n_{sp}\left[g(f)-1\right] f_b \sum_{k=2}^{m} \alpha^{k-2} l^{k-1} g(f)^{k-1}} \tag{S9}$$

Assuming the spectral envelope function $g(f)$ is flat in the RFSFL, $\alpha \times l \times g(f) \approx 1$, α equals 0.5, and the transition gain effect [S5, S6] of the EDFA is ignored. The SNR can be simplified as

$$\mathrm{SNR}_m = \frac{P_m}{8(m-1)a_0} = \frac{P_0 \tau_b}{8(m-1)Mt_b h\nu n_{sp}\left[g(f)-1\right] f_b} \tag{S10}$$

For each sub-channel of the SFC, the SNR deteriorates with increasing step number of the sub-stepped frequency.

Supplementary Note 4: Generation of electro-optic comb

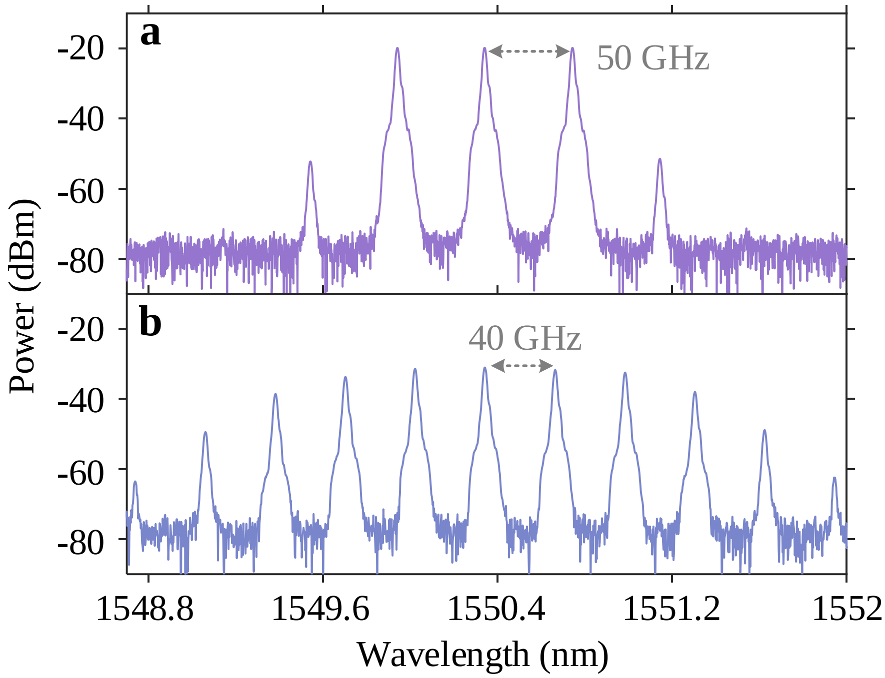

Fig. S2. Generation of electro-optic comb. a, Optical spectrum of a three-tone electro-optic comb with a comb interval of 50 GHz. **b,** Optical spectrum of a five-tone electro-optic comb with a comb interval of 40 GHz.

To generate both the SFC and the three-tone electro-optic comb, the same Mach-Zehnder modulators (MZM) are used. By properly adjusting the bias point of the MZMs [S7], a flat three-tone electro-optic comb with a comb interval of 50 GHz is generated, as shown in Fig. S2a. It should be noted that the comb number of the electro-optic comb is mainly limited by the frequency response of the MZMs and the maximum output power of the microwave source. By increasing the power of the driving signal or improving the frequency response of the MZMs, electro-optic combs with a higher comb number can be achieved. As an example, Fig. S2b shows a generated five-tone electro-optic comb with a comb spacing of 40 GHz.

Supplementary Note 5: Optical injection locking of the distributed feedback laser diode

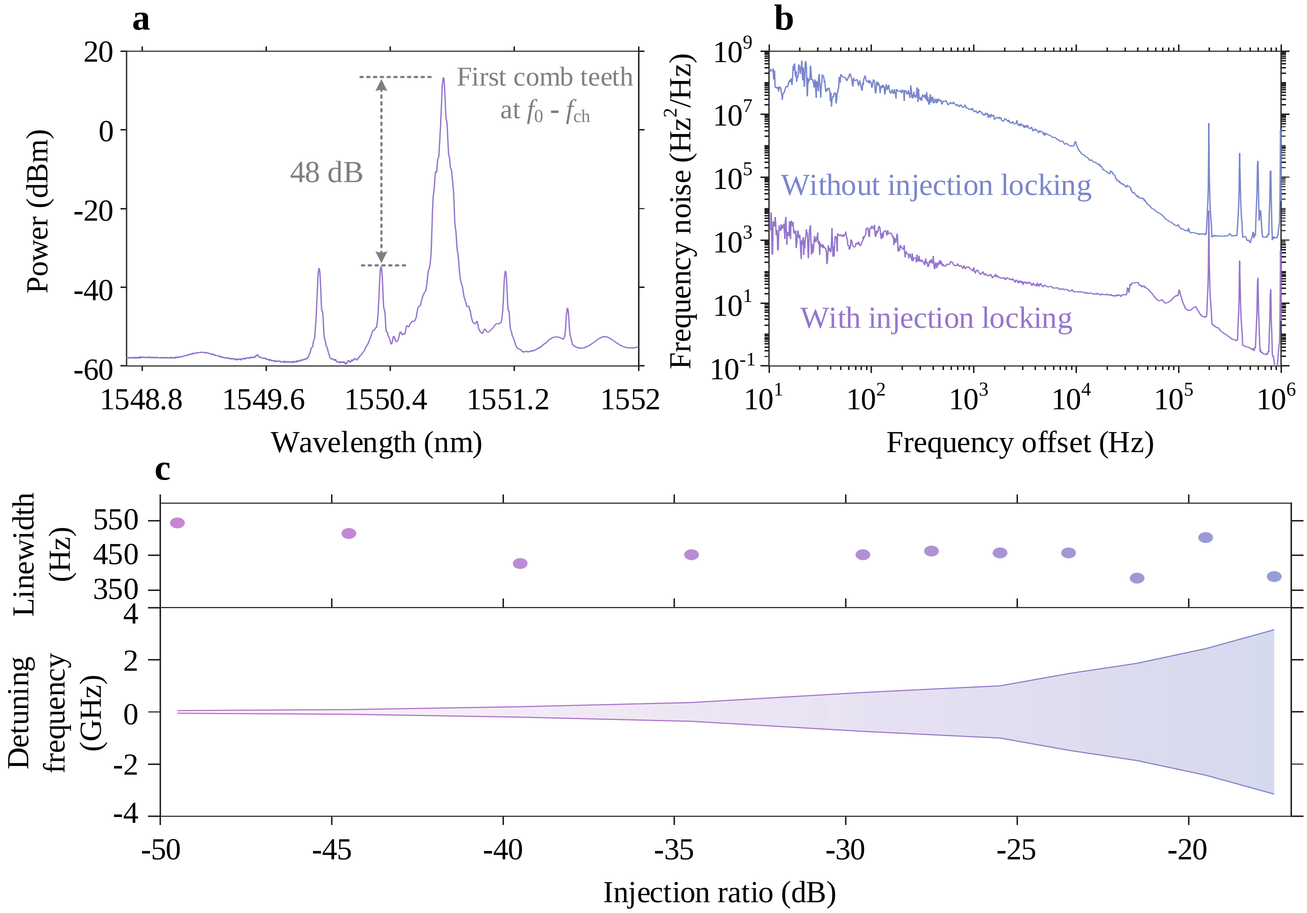

Fig. S3. Optical injection locking of the distributed feedback laser diode. a, Optical spectrum of the output from the DFB-LD after injection locking to the first comb teeth. **b,** Frequency noise of the output before and after injection locking. **c,** Dependence of the integrated linewidth and the detuning-frequency locking range on the injection ratio.

In this work, optical injection locking [S8] is employed to establish synchronization with a fixed frequency difference between the CW laser in the SFC path and the CW laser in the signal under test (SUT) reception path. Specifically, the three-tone electro-optic comb is injected into a distributed feedback laser diode (DFB-LD), which selects and amplifies the first comb tooth at f_0 - f_{ch}, as shown in Fig. S3a. The rejection ratio of the first comb teeth relative to the residual comb teeth is above 48 dB, indicating effective spectral selection.

The frequency noise of the output from the DFB-LD is shown in Fig. S3b, where the light blue and purple curves represent the frequency noise before and after injection locking, respectively. The corresponding integrated linewidths before and after injection locking are 33.496 kHz and 359 Hz, demonstrating a substantial reduction in frequency noise after injection locking. The effects of the injection ratio, defined as the ratio of the injected optical power to the output optical power, on the integrated linewidth and the detuning frequency locking range are shown in Fig. 3c. As the injection ratio increases, the detuning-frequency locking range becomes larger, while the integrated linewidth remains at the level of a few hundred hertz. These results confirm that optical injection locking can provide accurate frequency mapping in the proposed SFC advanced spectrum sensing system.

Supplementary Note 6: Image rejection of the SFC advanced spectrum sensing

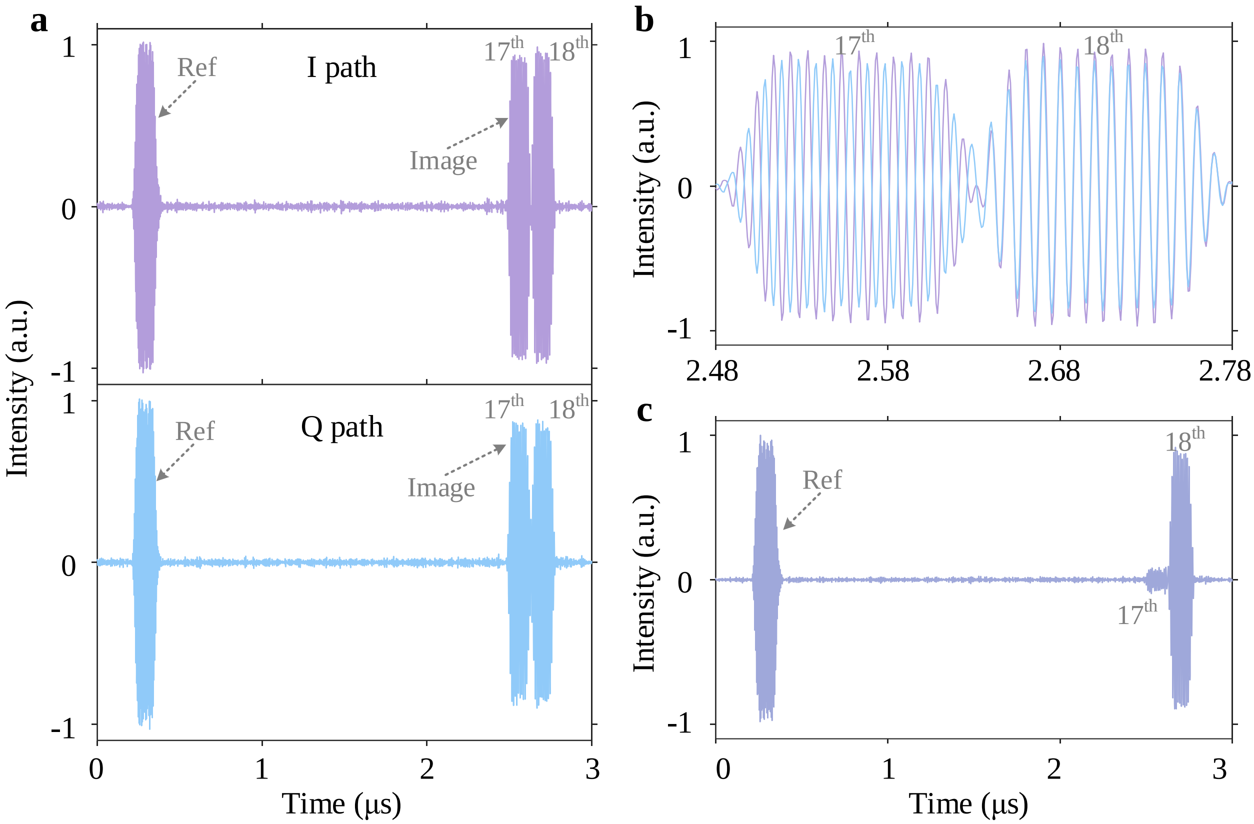

Fig. S4. Image rejection of the SFC advanced spectrum. a, Mapping temporal signals of the I and Q paths. **b,** Mapping temporal signals of the I and Q paths after coupling by a 90° electrical hybrid in the (k-1)th and kth time bins. **c,** The mapping temporal signal of the image-reject receiver.

Assuming the SUT optical signal is located in the first sub-channel, the first sub-channel stepped frequency optical signal, and the SUT optical signal are expressed as

$$\begin{aligned} E_{\mathrm{SF}}(t) &\propto \sum_{m=0}^{M-1} \mathrm{rect}\left(\frac{t-mt_b}{\tau_b}\right) \exp\left\{i2\pi\left[f_0 - f_{\mathrm{ch}} + (m+1) f_{\mathrm{b}}\right](t-mt_{\mathrm{b}})\right\} \\ E_{\mathrm{SUT}}(t) &\propto \exp\left[i2\pi\left(f_0 - f_{\mathrm{ch}} + f_{\mathrm{SUT}}\right)t\right] + \exp\left[i2\pi\left(f_0 - f_{\mathrm{ch}}\right)t\right] + \exp\left[i2\pi\left(f_0 - f_{\mathrm{ch}} - f_{\mathrm{SUT}}\right)t\right] \end{aligned} \quad \text{(S11)}$$

where f_{SUT} is the SUT frequency, the MZM2 for transforming the SUT ot optical domain is at the quadrature bias point.

The two optical signals are injected into a 90° optical hybrid, and the two outputs from the 90° optical hybrid are expressed as

$$\begin{aligned} E_I(t) &= E_{\mathrm{SF}}(t) + E_{\mathrm{SUT}}(t) \\ E_Q(t) &= E_{\mathrm{SF}}(t) + jE_{\mathrm{SUT}}(t) \end{aligned} \quad \text{(S12)}$$

The two optical signals are photoelectric detected with a bandwidth of f_{b}, respectively. The two mapping signals are expressed as

$$
\begin{aligned}
i_I(t) &\propto \mathrm{rect}\left(\frac{t}{\tau_\mathrm{b}}\right)\cos\left(f_\mathrm{b}t\right)+\mathrm{rect}\left(\frac{t-(k-1)t_b}{\tau_\mathrm{b}}\right)\cos\left(kf_\mathrm{b}t-f_\mathrm{ch}t\right) \\
&\quad +\mathrm{rect}\left(\frac{t-(k-2)t_b}{\tau_\mathrm{b}}\right)\cos\left[f_\mathrm{ch}t-(k-1)f_\mathrm{b}t\right] \\
i_Q(t) &\propto \mathrm{rect}\left(\frac{t}{\tau_\mathrm{b}}\right)\cos\left(f_\mathrm{b}t-\frac{\pi}{2}\right)+\mathrm{rect}\left(\frac{t-(k-1)t_b}{\tau_\mathrm{b}}\right)\cos\left(kf_\mathrm{b}t-f_\mathrm{ch}t-\frac{\pi}{2}\right) \\
&\quad +\mathrm{rect}\left(\frac{t-(k-2)t_b}{\tau_\mathrm{b}}\right)\cos\left[f_\mathrm{ch}t-(k-1)f_\mathrm{b}t+\frac{\pi}{2}\right]
\end{aligned} \tag{S13}
$$

The SUT frequency is assumed in the k^{th} time bin $[(k\text{-}1)t_\mathrm{b}, kt_\mathrm{b}]$, i.e., $(k\text{-}1)f_\mathrm{b} \le f_\mathrm{SUT} < kf_\mathrm{b}$. It can be seen that the image spur is observed in the $(k\text{-}1)^{th}$ time bin $[(k\text{-}2)t_\mathrm{b}, (k\text{-}1)t_\mathrm{b}]$, with an image frequency of f_b - f_Rx, where f_Rx is the extracted frequency in the k^{th} time bin. The detected I and Q paths in experiments are shown in Fig. S4a.

To suppress the image spurs, the two mapping outputs are coupled by a 90° electrical hybrid, and the detected Q path is phase shifted, as shown in Fig. S4b. The two coupled signals are combined and then filtered by a lowpass filter with a cutoff frequency of f_b. Finally, the output signal of the image-reject receiver is expressed as

$$
\begin{aligned}
i_{out}(t) &= i_I(t)+i_Q(t)\angle 90^\circ \\
&\propto \mathrm{rect}\left(\frac{t}{\tau_\mathrm{b}}\right)\cos\left(f_\mathrm{b}t\right)+\mathrm{rect}\left(\frac{t-(k-1)t_b}{\tau_\mathrm{b}}\right)\cos\left(kf_\mathrm{b}t-f_\mathrm{ch}t-\frac{\pi}{2}\right)
\end{aligned} \tag{S14}
$$

As can be seen, the image spur in the $(k\text{-}1)^{th}$ time bin is eliminated, and the experimental result is shown in Fig. S4c.

Supplementary Note 7: Voltage-frequency characteristic of the voltage control oscillator

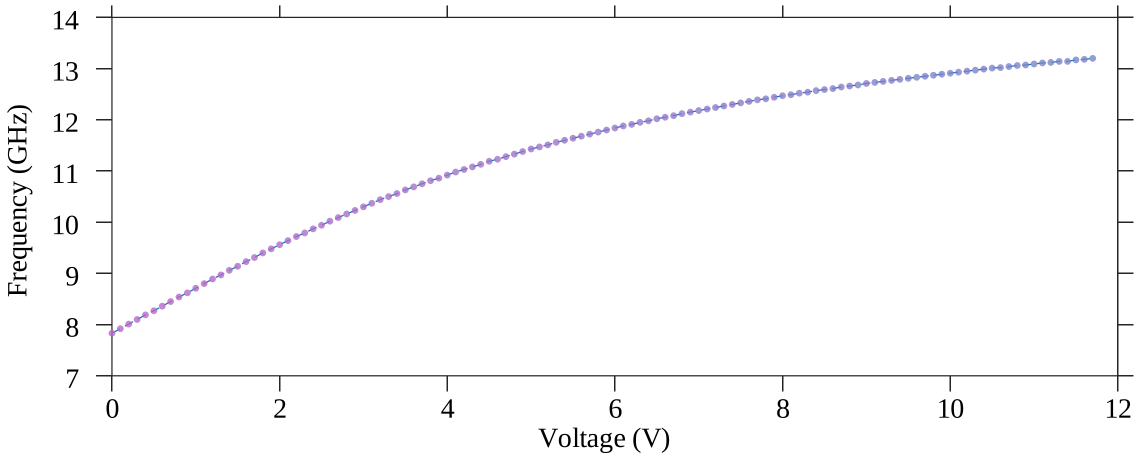

Fig. S5. Voltage-frequency characteristic of the voltage control oscillator.

Supplementary Note 8: Numerically calculated spectrograms and captured spectra of various SUTs

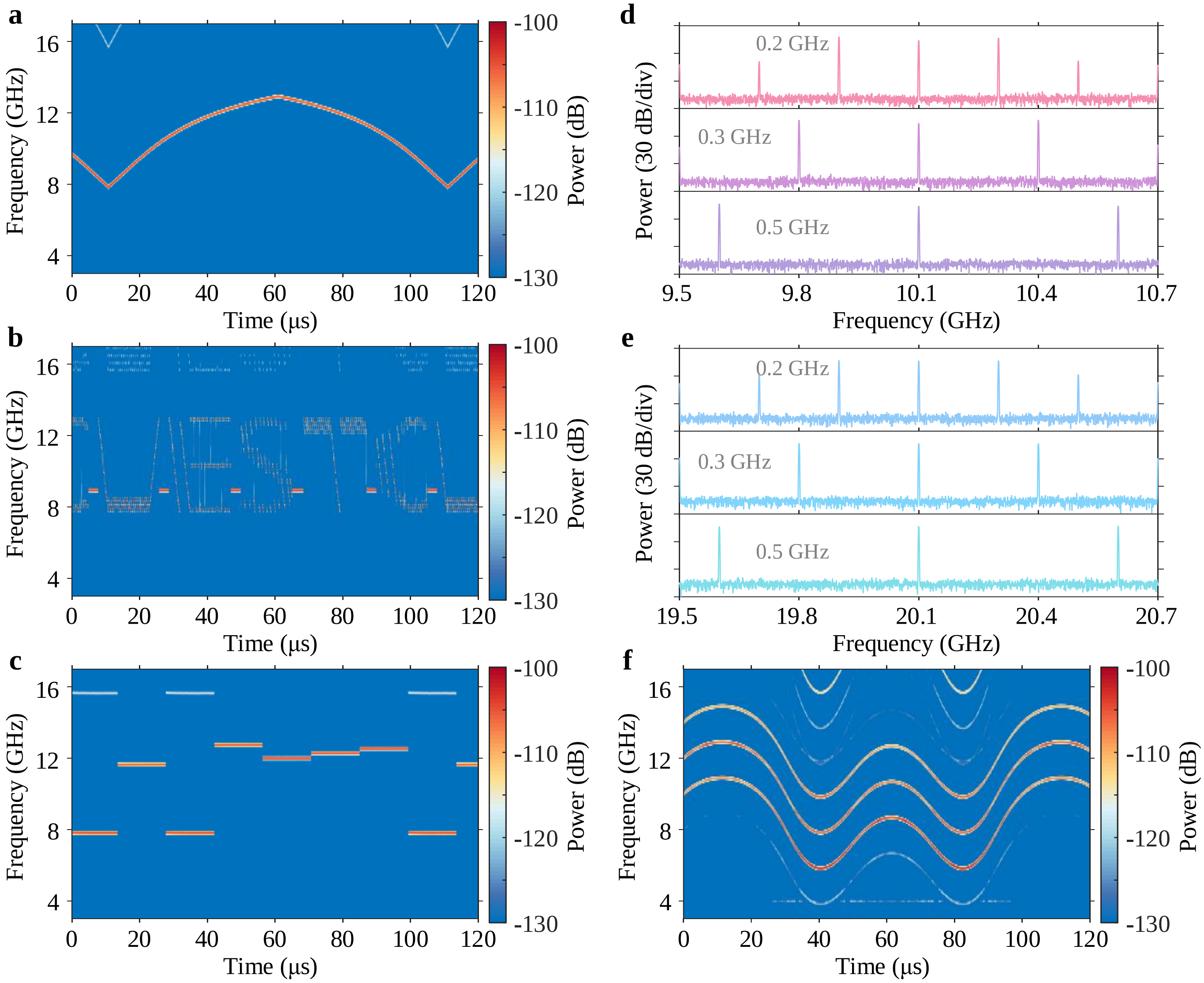

Fig. S6. Numerically calculated spectrograms and captured spectra of various SUTs. a, Spectrogram of a frequency-agile SUT with a triangular format. The nonlinearity arises from the non-ideal voltage-frequency characteristic of the voltage control oscillator. **b,** Spectrogram of a frequency-agile SUT with a "UESTC" format. **c,** Spectrogram of a frequency-agile SUT with a Costas-7 format. **d,** Spectrum of three-tone SUTs centered at 10.1 GHz with intervals of 0.2 GHz, 0.3 GHz, and 0.5 GHz. **e,** Spectrum of three-tone SUTs centered at 20.1 GHz with intervals of 0.2 GHz, 0.3 GHz, and 0.5 GHz. **f,** Spectrogram of a three-band frequency-agile SUT composed of nonlinear-chirp formats.

The numerically calculated spectrograms of various frequency-agile SUTs are shown in Figs. S6a to S6c. These spectrograms are obtained by applying the short-time Fourier transform (STFT) to temporal signals captured by a high-speed oscilloscope with a sampling rate of 80 GSa/s and a bandwidth of 20 GHz. By comparison with these reference spectrograms, the reconstructed results obtained with the proposed system show that the time-frequency information of all three types of frequency-agile SUT is recovered with high spectral completeness.

The spectra of the multi-tone SUTs, captured by a broadband electrical spectrum analyzer with a bandwidth of

50 GHz, are shown in Figs. S6d and S6e. By comparison with these reference spectra, the experimentally reconstructed results confirm accurate identification of the multi-tone frequency components. Correspondingly, the numerically calculated spectrogram of the multi-band frequency-agile SUT is shown in Fig. S6f. By comparison with this reference spectrogram, the reconstructed result demonstrates that the time-frequency information of the multi-band frequency-agile SUT is also recovered with high spectral completeness. Together, these results further verify the capability of the proposed SFC advanced spectrum sensing system for reconstructing complex frequency-agile, multi-tone, and multi-band signals.

Supplementary references

[S1] Zhang, Z., Liu, Y., Stephens, T. et al. Photonic radar for contactless vital sign detection. *Nat. Photon.* **17**, 791-797 (2023)

[S2] Fernández-Pousa, C. R. & De Chatellus, H. G. Fundamental SNR limits imposed by ASE in frequency-shifting loops. *J. Lightwave Technol.* **40**, 6831-6844 (2022).

[S3] Kanagaraj, N. et al. Optimization of acousto-optic optical frequency combs. *Opt. Express* **27**, 14842 (2019).

[S4] Nguyen, T. A. et al. Photonic radio frequency memory using frequency shifting recirculating delay line structure. *J. Lightwave Technol.* **32**, 99-106 (2014).

[S5] Zhang, J., Yi, L., & Li, Y. A theoretical model for recirculating frequency-shifted fiber loop supporting ultra-large number of circulations. *J. Lightwave Technol.* **43**, 7163-7171 (2025).

[S6] Wang, G., Song, C., Yuan, Q. et al. Optical RF memory with an ultra-long storage time of 13 ms. *Photonics Res.* **14**, 552-559 (2026)

[S7] Li, X. et al. Photonic generation of a tunable multi-band linearly frequency-modulated waveform. *Opt. Commun.* **553**, 130117 (2024).

[S8] Wang, Y. et al. Millihertz-linewidth self-injection–locked semiconductor laser based on a hollow FP cavity. *Opt. Lett.* **50**, 9-12 (2025).